J Mater Sci: Mater Electron (2017) 28:4654–4660
DOI 10.1007/s10854-016-6104-y

Influence of sintering temperatures of ceramic targets on microstructures and photoelectric properties of titanium-doped ZnO nano-films

Zhenying Chen[1,2] · Fei Li[1] · Xiaowei Chen[1] · Shoulei Xu[1] · DingKang Xiong[1] · YuYang Huang[1] · Wen Deng[1]

Received: 3 October 2016 / Accepted: 17 November 2016 / Published online: 22 November 2016
© Springer Science+Business Media New York 2016

Abstract Thin films of Ti-doped ZnO (TZO) were prepared by RF magnetron sputtering using targets prepared with sintering temperatures in the range 1100–1500 °C; the microstructures and optoelectronic properties of the TZO targets and films were characterized by SEM, XRD, Hall Effect analysis, UV–VIS spectrophotometry and physical property measurement system. Results indicated that the target sintering temperature affected both the TZO targets and films. The Ti/Zn atomic ratios in the targets decreased progressively with increasing sintering temperature, but by a smaller amount in films prepared from them. XRD patterns showed that all films were preferentially oriented along the c axis at $2\theta \sim 34°$ in their XRD patterns. The films sputtered with targets sintered at above 1300 °C were relatively smooth, and had larger average grain size. The target sintered at 1450 °C had the highest density. The best optoelectronic properties were found with the film sputtered from the target sintered at 1300 °C; this sample had superior crystal properties, high average optical transmittance (88.9%), and the lowest resistivity (8.47×10^{-4} Ω cm). Furthermore, the resistivity of all the films changed with temperature between 10 and 350 K, they experienced an initial decrease followed by an increase as the temperature was raised.

✉ Wen Deng
wdeng@gxu.edu.cn

[1] College of Physical Science and Engineering, Guangxi University, Nanning 530004, Guangxi, People's Republic of China

[2] Xingjian College of Arts and Sciences, Guangxi University, Nanning 530004, Guangxi, People's Republic of China

1 Introduction

Transparent conductive oxide (TCO) thin films with a wide band gap, low resistivity, and high transmittance are widely used in solar cells, displays, and other optoelectronic devices. Tin-doped indium oxide (ITO) is the most widely used in industry, but indium posses toxicity problems, and is relatively rare. Therefore, ZnO is potentially a good substitute for ITO, because of its comparable optoelectronic properties, relative abundance, ease of doping, and high stability; it has also been extensively investigated.

The optoelectronic properties of ZnO transparent conductive films can be improved by doping with a small amount of an impurity, such as Al, Ga, In, V, Nb, Mo, Mg, Bi, or B, and there are many publications on Al-doped ZnO [1–13]. In Ti-doped ZnO, XPS results have indicated that Ti^{4+} ions replace Zn^{2+} ions in the TZO films [14]. If Ti^{4+} ions replace the Zn^{2+} ions in the zinc oxide lattice, more free electrons can be provided. And this will increase the carrier concentration and conductivity. Therefore, it is important to comprehensively investigate the physical properties of TZO films in order to fully understand their potential uses and applications. The microstructures and optoelectronic properties of TZO films have been the subject of a few investigations with respect to the thickness of the TiO_2 buffer layer [15], sputtering power [14], substrate temperature [16], annealing temperature [15, 17], and hydrogen plasma surface treatment [18]. Many of these reports have focused on the sputtering and post treatment technology, and only a few have considered the influence of target technology on the optoelectronic properties of films. Therefore, the aims of the present work were to investigate the influence of target sintering temperature on the properties of TZO films, to find the best sintering temperature for desirable optimal optoelectronic properties.

2 Experimental procedures

TZO target materials with TiO_2 contents of 2.1 at% were prepared by a solid-state reaction method using ZnO and TiO_2 nano powder (obtained from Aladdin Co., Ltd.) as raw materials; both were reported to have 99.99% purity. The two powders were mixed with ultrapure water in a magnetic stirrer for 10 h and then were dried in an oven. The mixture was then pressed into 6 tablets using a powder compressing machine, and the samples sintered at 1100, 1200, 1300, 1400, 1450, and 1500 °C for 4 h in a muffle furnace, respectively. The resulting cylindrical TZO ceramic targets had about 60 mm diameter and 3 mm thickness.

Thin films of the 6 TZO targets were deposited on glass substrates by the RF magnetron sputtering method using a double chamber magnetron sputtering system produced by the Chinese Academy of Sciences. Microslides were used as the substrates, which were cleaned using three sequential ultrasonic baths (acetone, anhydrous ethanol, and ultrapure water) for 10 min. Then the slides were flushed with ultrapure water, dried in a 70 °C oven, and coated in the sputtering chamber. The coating process parameters were set as follows: base pressure 5.0×10^{-5} Pa, sputtering power 150 W, target distance 60 mm, sputtering gas 99.995% high-purity Ar, and substrate temperature 150 °C. A pre-sputtering stage was run for 30 min before coating to eliminate impurities on the target surface, and the deposition time for each sample was 70 min. Six samples were marked corresponding to target sintering temperature 1100, 1200, 1300, 1400, 1450, and 1500 °C, respectively.

The structural, morphological and photoelectrical properties of the TZO targets and films were then investigated in detail. Photos describing the color, and target shape were taken with a digital camera. The diameters of targets before and after sintering were measured with a vernier caliper, and the densities of them were abtained using an electronic hydrometer according to the Archimedes law (DahoMeter DE-120 M). The microstructure and growth orientation of the TZO targets and films were characterized by XRD using Cu Kα radiation ($\lambda = 1.5406$ Å) in a X-ray diffractometer (Dandong Haoyuan Instrument Co., Ltd., China). The surface morphology and EDS analysis of the targets and films were studied using SEM (Hitachi, Model S-3400 N) and FE-SEM (Hitachi, Model SU8020). The film thickness was measured using profilometer (Bruker, DektakXT). The optical transmission was evaluated by UV–VIS spectrophotometer (Shimadzu, UV-2700). The electric properties of the films were tested at room temperature using a Hall Effect analyzer (SWIN, HALL8800), and their resistivity measured at various temperatures using the electrical transport measurement option of physical property measurement system (Quantum Design Company, PPMS-9).

3 Results and discussion

3.1 Microstructures of the targets

Because of increased sintering shrinkage with increasing sintering temperature and the size limitation (56.0–66.5 mm) of the magnetron sputtering target, the diameters of the ceramic bodies before sintering at 1100–1400 °C were 68 mm, whereas they were 70 mm in the others. Before sintering all of the targets were white, but as shown in the digital photos (Fig. 1), shrinkage in diameter (Table 1), target density (Fig. 2), and SEM morphology (Fig. 3), the sintering temperature had a large influence on the color, shrinkage, compactness and uniformity of the targets. Targets sintered at temperatures ≤1300 °C remained white in color with a loose structure, small size shrinkage, and poor sintering quality. With an increase in sintering temperature from 1300 to 1450 °C, the target color gradually deepened and to a uniform gray-green, the size shrinkage and density gradually increased, resulting in a decrease in the size and density of pores, and a progressive improvement in the sintering quality. The optimum target density (5.67 g cm^{-3}) was achieved with the sample sintered at 1450 °C, but the sintering quality deteriorated slightly as the sintering temperature was increased to 1500 °C, and an oversintering phenomenon occurred.

The XRD patterns of the TZO targets were shown in Fig. 4. The majority of the peaks were assigned to ZnO particles, but minor amounts of a new spinel phase, $Zn(ZnTi)O_4$, were also generated in the sintering process in amounts that increased with increasing sintering temperature. No TiO_2 phase was observed in the target XRD patterns, thus indicating that the other Ti ions were probably substituted in the ZnO crystal lattice.

Analyses of the compositions of the TZO targets by EDS at seven different places of each sample indicated that there was only a very small difference between the measured values. The atomic Ti/Zn ratios in the targets were shown in Fig. 5. For sintering temperatures ≥1300 °C, the atomic Ti/Zn ratios were progressively lower than in the starting materials (2.1 at%). This could be the consequence of the greater volatility of TiO_2 than ZnO, because the melting point of TiO_2 (1843 °C) was lower than that of ZnO (1975 °C).

3.2 Microstructures of thin films

As shown in Fig. 2, progressive increase in thickness and growth rate of the TZO films was observed as the target sintering temperature was increased from 1100 to 1450 °C, followed by a small decrease at 1500 °C. As described

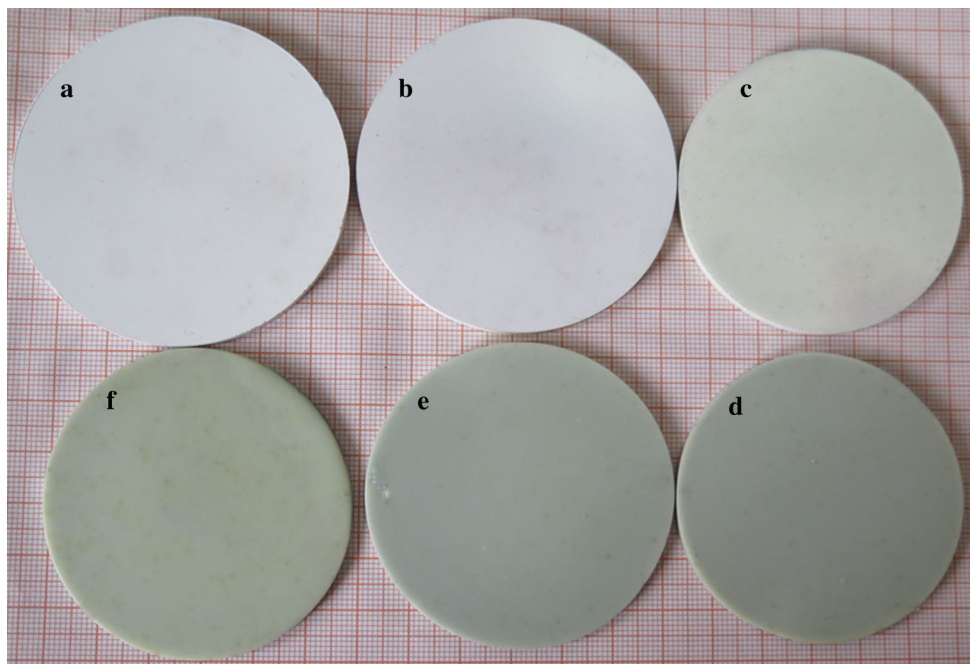

Fig. 1 Photographs of TZO targets with different sintering temperatures. **a** 1100 °C, **b** 1200 °C, **c** 1300 °C, **d** 1400 °C, **e** 1450 °C, **f** 1500 °C

Table 1 Changes in TZO target diameters before and after sintering

Sintering temperature (°C)	1100	1200	1300	1400	1450	1500
Diameter before sintering (mm)	68.00	68.00	68.00	68.00	70.00	70.00
Diameter after sintering (mm)	66.13	62.60	56.32	56.19	60.52	60.49
Diameter shrinkage value (mm)	1.87	5.40	11.68	11.81	9.48	9.51
Diameter shrinkage ratio (%)	2.75	7.94	17.18	17.36	13.54	13.59

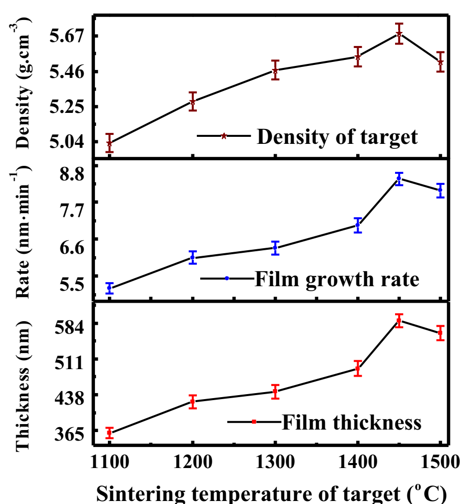

Fig. 2 Densities of target, thicknesses of films and growth rates of TZO films

above, the targets increased in density and uniformity as the sintering temperature was increased from 1100 to 1450 °C, and the rate of particles sputtering from the targets would be correspondingly increased; the film thickness increased from 360 to a maximum of 588 nm, and the deposition rate increased from 5.14 to a maximum of 8.4 nm min^{-1}. At higher target sintering temperature (1500 °C), oversintering made it more difficult for the particles to be sputtered out, and the sputtering rate decreased. The atomic Ti/Zn ratios in the films was reduced with increasing sintering temperature by a lower amount than in the corresponding targets (see Fig. 5), this indicated that the sputtered efficiencies of Ti atom is higher than that of Zn atom, that is, Ti atom can be sputtered out from target and deposited on substrate more easily than Zn atom.

The XRD patterns of all of the TZO films (Fig. 6) exhibited a strong diffraction peak at $2\theta = 34.42°$, which corresponded to the ZnO (002) crystal plane and had the lowest surface free energy. This indicated that the films were preferentially oriented along the c-axis. No peaks from neither TiO_2 nor Zn_2TiO_4 was observed in the 20°–80° range, thus verifying that most of Ti^{4+} ions were substituted in the ZnO crystal lattice. The (002) peak intensity was first increased then decreased with increasing target sintering temperature (Fig. 6). Measurements of the (002) peak full-width at half maximun (FWHM) (Fig. 7)

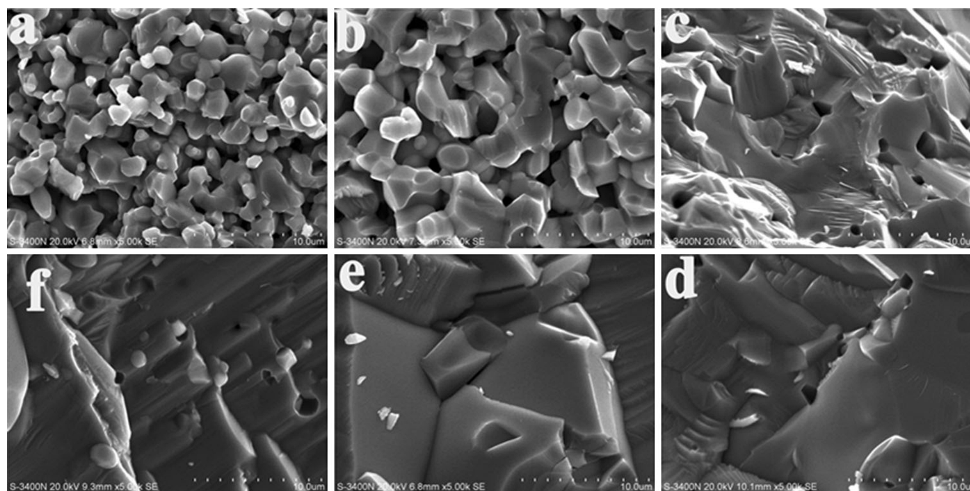

Fig. 3 SEM micrographs of TZO targets. **a** 1100 °C, **b** 1200 °C, **c** 1300 °C, **d** 1400 °C, **e** 1450 °C, **f** 1500 °C

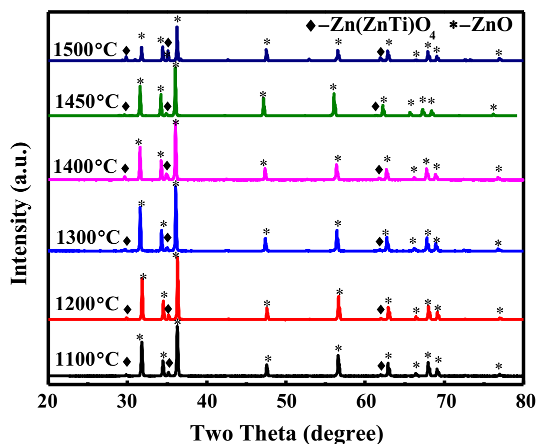

Fig. 4 XRD patterns of TZO targets with different sintering temperatures

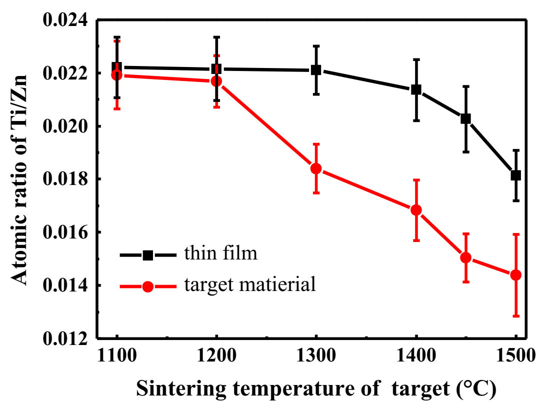

Fig. 5 Atomic ratios of Ti/Zn in TZO targets and thin films

and calculation of the average grain size using the Seherrer formula [14, 19] indicated that the grain size first increased then decreased with increasing target sintering temperature. Optimum crystallinity was achieved with the film prepared

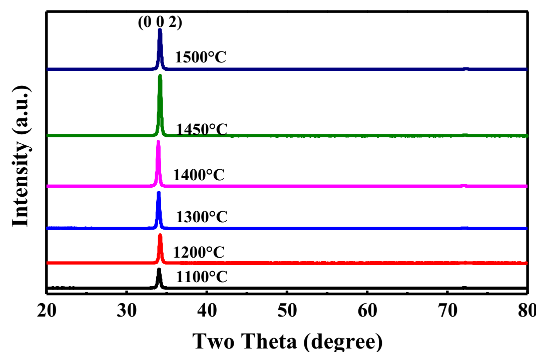

Fig. 6 XRD patterns of TZO films

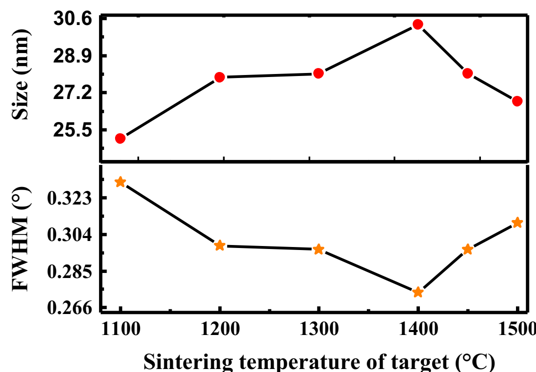

Fig. 7 FWHM of XRD patterns and grain sizes of TZO films

from the target sintered at 1400 °C which had the higher intensity of peak, the smallest peak FWHM, and the largest average grain size of 30.3 nm.

The surface morphology features of the TZO films revealed by SEM (Fig. 8) showed that films prepared from targets with sintering temperatures <1200 °C were not uniform and had a smaller average grain size, and thus produced unsatisfactory films. The crystal morphology of

films from targets with sintering temperatures ≥1200 °C were more compact and uniform. The grain size in the film increased first with increasing target sintering temperature, and reached maximum at 1400 °C, then decreased with increasing target sintering temperature. And it was consistent with the XRD results (Fig. 7).

3.3 Photoelectrical properties of the thin films

The transmission spectra for the TZO films between 300 and 800 nm were shown in Fig. 9, and their average transmittance in the visible region (400–760 nm) in Table 2. Each TZO film exhibited high transparency (>86%) with little difference between films.

Measurements using a Hall Effect analyzer showed that the target sintering temperature influenced the electrical properties of the TZO films (Table 3). The minimum value for the resistivity (8.47×10^{-4} Ω cm) was observed with the TZO film prepared from the target sintered at 1300 °C, which also had the highest carrier concentration and mobility. These could result from a number of factors, including the larger average grain size, denser surface and lower defect concentration, which would decrease the number of traps for the carriers. On the other hand, replacement of Zn^{2+} ions by Ti^{4+} ions in the ZnO lattice would provide more free electrons and thus increased carrier concentration. The more Ti^{4+} ions replacing Zn^{2+} ions in the film, the higher carrier concentration, but the lattice distortion could lead to deterioration in mobility.

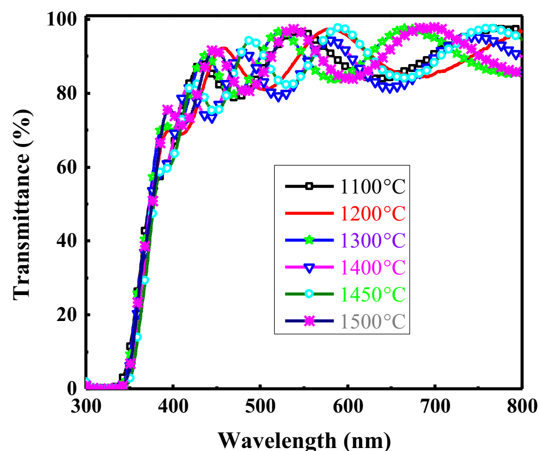

Fig. 9 Optical transmittance spectra of TZO films

Thus the lowest resistivity for the film prepared from the target sintered at 1300 °C may be attributed to a combination of the better crystallization than the films from targets sintered at 1100 and 1200 °C (Fig. 8), and the higher replacement rate of titanium atoms and smaller lattice distortion than the films from targets sintered at 1400–1500 °C (Fig. 5).

Optical band gap values (Eg) of TZO films were obtained by extrapolating the linear region of the $(\alpha E)^2-E$ curve to $(\alpha E)^2 = 0$ [14, 17, 20, 21], and the results for all films were shown in Fig. 10. The optical energy gaps in all of the TZO films were larger than that of pure ZnO (3.37 eV). This phenomenon was mainly caused

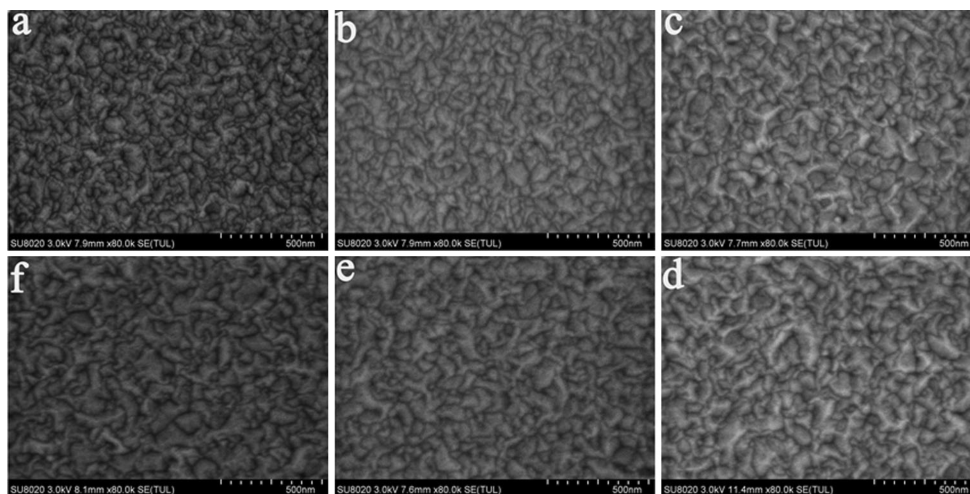

Fig. 8 SEM micrographs of TZO thin films. **a** 1100 °C, **b** 1200 °C, **c** 1300 °C, **d** 1400 °C, **e** 1450 °C, **f** 1500 °C

Table 2 Average optical transmittances of TZO films in wavelength from 400 to 760 nm (%)

The sintering temperature (°C)	1100	1200	1300	1400	1450	1500
The average transmittance (%)	87.83	87.07	88.82	86.92	87.51	89.14

Table 3 Parameters from hall effect measurements for TZO films

Target sintering temperature (°C)	Electrical resistivity (10^{-4} Ω cm)	Carrier concentration (10^{20}cm^{-3})	Carrier mobility (cm^2 v^{-1} s^{-1})
1100	14.98	2.59	16.11
1200	14.66	2.62	16.28
1300	8.47	3.08	23.97
1400	8.86	2.92	24.18
1450	9.22	2.91	23.31
1500	9.51	2.85	23.06

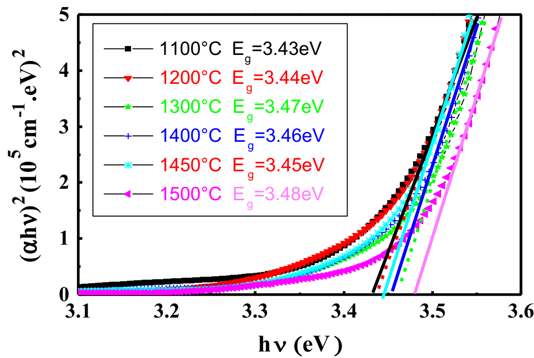

Fig. 10 Plots of $(\alpha h\nu)^2$ versus photon energies (hν) of TZO films

by the Burstein-Moss shift, the replacement of Zn^{2+} ions by Ti^{4+} ions in the ZnO lattice would provide more free electrons and thus increase carrier concentration. When the electron concentration exceeds a critical value, the electrons would fill in the bottom of the conduction band, causing that the electron transitions from the valence band to the conduction band require more energy from a photon absorbed than that in the intrinsic ZnO semiconductors. And those of the films from targets sintered at 1300 °C (3.47 eV) and 1500 °C (3.48 eV) were larger than the other films. Possible explanations for this phenomenon were: (i) superior film crystallization could reduce carrier capturing and scattering, leading to a higher carrier concentration. (ii) Replacement of Zn^{2+} with Ti^{4+} resulted in a further increase in carrier concentration. And (iii) the larger carrier concentration fills the lowest energy level in the conduction band and caused a Burstein-Moss displacement effect, resulting in the Fermi level entering the conduction band, and increasing the optical bandgap [22].

Results from measurements of the temperature dependence of the resistivity (10–350 K) in the films by PPMS

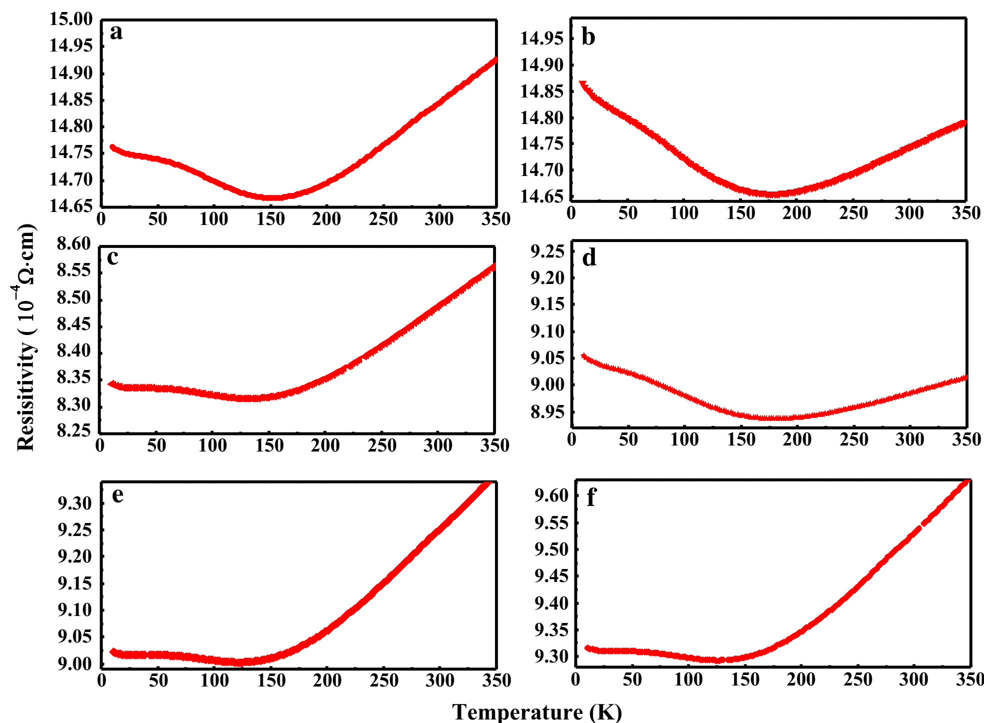

Fig. 11 Resistivities versus temperatures of TZO thin films. **a** 1100 °C, **b** 1200 °C, **c** 1300 °C, **d** 1400 °C, **e** 1450 °C, **f** 1500 °C

(Fig. 11) showed agreement between the values at room temperature and those in Table 2. The resistivity of all the films changed with temperature between 10 and 350 K, they experienced an initial decrease followed by an increase as the temperature was raised, for example, the resistivity of the film prepared from the target sintered at 1300 °C had a minimum value of $8.316 \times 10^{-4}\ \Omega$ cm around 146 K. The optical bandgap of the TZO film prepared from the target sintered at 1300 °C was relatively large ($\sim$3.47 eV), excitation was based on impurity excitation in the temperature range 10–146 K; intrinsic excitation and the effect of lattice vibrations were negligible, and the carriers were contributed mainly by donor ionization. Excitations of impurities were increased with increasing temperatures, leading to an increase in the carrier concentration and conductivity. However, the carrier concentration reached saturation, and resistivity was a minimum at 146 K. Above 146 K, lattice vibrations begin to have an impact, although intrinsic excitation is still not significant because of the wide bandgap. However, lattice vibrations enhanced the carrier scattering, and resulted in an increase in resistivity. A similar trend was observed for the other films, which all showed an initial decrease followed by an increase as the temperature increased.

4 Conclusions

TZO films were prepared by RF magnetron sputtering using targets with different sintering temperatures. The microstructures and optoelectronic properties of both TZO targets and films were characterized by XRD, SEM, Hall Effect analysis, UV–VIS spectrophotometry and PPMS-9. The results indicated that the target sintering temperature affects the TZO targets and films. ZnO was the main component of the targets, but the Ti/Zn atomic ratio gradually decreased with increasing sintering temperature. XRD patterns showed that all films had a (002) preferential orientation along the c axis at $2\theta \sim 34^{\circ}$. The Ti/Zn atomic ratio in the film was higher than that in corresponding target for sintering temperatures $\geq$1300 °C. Films sputtered with targets sintered at 1300–1450 °C had relatively smoother, denser surfaces, and larger average grain sizes than those sintered at other temperatures. The best optoelectronic properties were found with the film sputtered from the target sintered at 1300 °C, because this film had superior crystallization, with high average optical transmittance (88.9%), and the lowest resistivity of $8.47 \times 10^{-4}\Omega$ cm. Furthermore, the resistivities of all the films changed with temperature between 10 and 350 K, they decreased initially then increased at the temperature increased.

Acknowledgements The authors thank Professor Dr. Bernard A. Goodman for his helpful discussions. This work was supported by the National Natural Science Foundation of China (Grant Nos.112650020 and 11675043), and Foundation of Xingjian College of Guangxi of University China (Grant No. 2016ZKA01).

References

1. B. Onwona-Agyeman, M. Nakao, T. Kohno, D. Liyanage, K. Murakami, T. Kitaoka, Chem. Eng. J. **219**, 273 (2013)
2. Q. Huang, Y.F. Wang, S. Wang, D.K. Zhang, Y. Zhao, X.D. Zhang, Thin Solid Films **520**, 5960 (2012)
3. M.H. Jiang, X.Y. Liu, H. Wang, Surf. Coat. Technol. **203**, 3750 (2009)
4. J.Y. Kao, C.Y. Hsu, G.C. Chen, D.C. Wen, J. Mater. Sci.: Mater. Electron. **23**, 1352 (2012)
5. Q.B. Ma, H.P. He, Z.Z. Ye, L.P. Zhu, J.Y. Huang, Y.Z. Zhang, B.H. Zhao, J. Solid State Chem. **181**, 525 (2008)
6. S. Okuda, T. Matsuo, H. Chiba, T. Mori, K. Washio, Thin Solid Films **557**, 197 (2014)
7. L.P. Peng, L. Fang, X.F. Yang, Q.L. Huang, F. Wu, Y.C. Cao, M.W. Li, C.Y. Kong, Int. J. Mod. Phys. B **25**, 995 (2011)
8. L.P. Peng, L. Fang, X.F. Yang, H.B. Ruan, Y.J. Li, Q.L. Huang, C.Y. Kong, Phys. E.: Low-Dimens. Syst. Nanostruct. **41**, 1819 (2009)
9. H. Qin, H.F. Liu, Y.Z. Yuan, Surf. Eng. **29**, 70 (2013)
10. S. Wang, J. Shen, Z.J. Zhang, X.L. Yang, Q. Zhang, J. Vac. Sci. Technol. **28**, 1 (2008)
11. H.W. Wu, R.Y. Yang, C.M. Hsiung, C.H. Chu, J. Mater. Sci.: Mater. Electron. **24**, 166 (2013)
12. J.W. Xu, H. Wang, M.H. Jiang, X.Y. Liu, Bull. Mater. Sci. **33**, 119 (2010)
13. H.F. Zhang, R.J. Liu, H.F. Liu, Q.S. Chen, X.F. Wang, Y.X. Mei, J. Synth. Cryst. **39**, 766 (2010)
14. H.X. Chen, W.G. Guo, J.J. Ding, S.Y. Ma, Superlattices Microstruct. **51**, 544 (2012)
15. Y.C. Lin, C.Y. Hsu, S.K. Hung, D.C. Wen, Ceram. Int. **39**, 5795 (2013)
16. S.S. Lin, J.L. Huang, D.F. Lii, Mater. Chem. Phys. **90**, 22 (2005)
17. H.P. Chang, F.H. Wang, J.C. Chao, C.C. Huang, H.W. Liu, Curr. Appl. Phys. **11**, S185 (2011)
18. F.H. Wang, H.P. Chang, J.C. Chao, Thin Solid Films **519**, 5178 (2011)
19. J. Liu, S.Y. Ma, X.L. Huang, L.G. Ma, F.M. Li, F.C. Yang, Q. Zhao, X.L. Zhang, Superlattices Microstruct. **52**, 765 (2012)
20. K. Bergum, P.A. Hansen, H. Fjellvag, O. Nilsen, J. Alloys Compd. **616**, 618 (2014)
21. W.S. Liu, S.Y. Wu, C.H. Tseng, C.Y. Hung, Thin Solid Films **570**, 568 (2014)
22. L. Gao, Y. Zhang, J.M. Zhang, K.W. Xu, Appl. Surf. Sci. **257**, 2498 (2011)